The Nucleus ***63***, *No. 2 (2026) 1-9*

https://doi.org/10.71330/thenucleus.2026.1520

www.thenucleuspak.org.pk

The Nucleus

ISSN 0029-5698 (Print)
ISSN 2306-6539 (Online)

Structural, Electronic, Magnetic, and Thermoelectric Properties of Cr-Doped Double Perovskites Cs_2GeX_6 (X = Cl, Br): DFT Calculations

Sultan Abbas, M. Aslam Khan*, Shanawer Niaz

Institute of Physics, Khwaja Fareed University of Engineering and Information Technology, 64200, Rahim Yar Khan, Pakistan

ABSTRACT

Physical properties of chromium-doped halide double perovskites (DPs) Cs_2GeX_6 (X = Cl, Br) are investigated using density functional theory (DFT) as implemented in the WIEN2k code. These materials are of interest for solar cells and photovoltaics owing to their non-toxicity and ecological sustainability. The structural, electronic, magnetic, and thermoelectric characteristics of pristine and Cr-doped A_2BX_6 (A = Cs; B = Ge; X = Cl, Br) halides are examined. The negative formation energies and the tolerance factors confirm the thermodynamic and structural stability of these compounds. The band gap of Cs_2GeCl_6 is 4.5 eV and that of the doped $Cs_2Ge_{0.75}Cr_{0.25}Cl_6$ is 4.1 eV, whereas the band gap of Cs_2GeBr_6 is 3.0 eV and that of the doped $Cs_2Ge_{0.75}Cr_{0.25}Br_6$ is 2.5 eV. $Cs_2Ge_{0.75}Cr_{0.25}Cl_6$ and $Cs_2Ge_{0.75}Cr_{0.25}Br_6$ exhibit an indirect band gap in the spin-up channel and a direct band gap in the spin-down channel. Cr doping increases the equilibrium lattice parameters of Cs_2GeCl_6 and Cs_2GeBr_6 (Cs_2GeCl_6: 10.32 Å, $Cs_2Ge_{0.75}Cr_{0.25}Cl_6$: 10.55 Å, Cs_2GeBr_6: 10.65 Å, and $Cs_2Ge_{0.75}Cr_{0.25}Br_6$: 10.85 Å). Both Cr-doped compounds, $Cs_2Ge_{0.75}Cr_{0.25}Cl_6$ and $Cs_2Ge_{0.75}Cr_{0.25}Br_6$, possess the same integer total magnetic moment of 3 μ_B, indicating ferromagnetic semiconducting behavior. The thermoelectric properties were evaluated in terms of the electrical conductivity, electronic thermal conductivity, Seebeck coefficient, and power factor. The computed power factors (PF/τ) at 200 K are $1.90\times 10^{11} W/K^2ms$ and $1.85\times 10^{11} W/K^2ms$, and $3.98\times 10^{11} W/K^2ms$ and $4.09\times 10^{11} W/K^2ms$ at 800 K for $Cs_2Ge_{0.75}Cr_{0.25}Cl_6$ and $Cs_2Ge_{0.75}Cr_{0.25}Br_6$, respectively. The positive Seebeck coefficients indicate p-type conduction, and the room-temperature ZT values of 0.79 and 0.78 highlight the potential of these materials for thermoelectric applications.

Keywords: *Cr-doping, Structural property, Electronic property, Thermoelectric property, Magnetic property, Density functional theory*

1. Introduction

The recently obtained results show that double halide perovskites are promising materials for luminescence and photovoltaics. Despite great progress in materials science, a problem remains in accurately defining "perovskite." Therefore, perovskite materials are defined here with the additional specification of "heavier halides," i.e., Cl, Br, and I. It is necessary to specify the distinguishing features of halide perovskites within this definition and point out crystal structures that are not regarded as perovskites despite being close to this class in terms of structural characteristics [1]. The rapid growth of the world population, combined with the use of modern electronics and other technologies, leads to a constant need for energy that is hardly supplied using conventional sources. Therefore, much work has focused on improving the efficiency of various renewable technologies [2, 5], including thermoelectric devices and solar cells. To improve the performance of solar cells and other photovoltaic devices, properties of halide double perovskite materials should be optimized [6, 10]. Double halide perovskites are considered highly efficient and reliable materials in solar cells and photovoltaics [11, 12]. They exist as organic–inorganic and purely inorganic perovskites, but double perovskites are mostly produced from the inorganic composition of the mentioned compounds. Their unusual structure and physical properties make them of great interest in materials science research [13]. Initially, organic–inorganic halide perovskites were employed as sensitizers in dye-sensitized solar cells (DSSCs), but their low efficiency and poor stability limited large-scale application [14, 15].

Subsequent research has shown that using inorganic halide double perovskite (HDP) materials can increase device efficiency and stability. For example, several investigations compare the efficiency of HDP-based solar cells with that of traditional silicon-based photovoltaics [16]. Halide double perovskites can also be used in thermoelectric generators to recover waste heat produced by commercial electronic and mechanical equipment. The Pb-free double perovskites A_2BX_6 (e.g., A = K, Rb, Cs; B = Ge) are promising materials for renewable energy and alternatives to hybrid halide perovskites [17]. In conventional halide perovskites, Pb has long been regarded as indispensable for achieving high device efficiency and stability. Lead is highly poisonous and can threaten people's health [18]. A further disadvantage of Pb-based perovskites is their instability under long-term solar irradiation. Double halide perovskites are among the most promising compounds for solar cells and similar technologies and will most likely be used to manufacture lasers, solar cells, photovoltaic absorbers, and light-emitting diodes [19]. That is why scientists strive to replace Pb with other elements, such as Ge^{2+} and Sn^{2+}, which are more environmentally friendly and can improve efficiency and stability. However, these divalent ions are unstable because they are easily oxidized to the 4+ state [20, 21]. Replacing Pb^{2+} with Bi^{3+} and Sb^{3+} does not improve performance [22, 23]. The future of these materials may lie in homovalent [24] and heterovalent [25] substitution.

The formation of a direct bandgap is another commonly observed characteristic of double perovskite halides. Their properties can be tuned by controlling the stoichiometric ratio between the constituent elements [26, 28]. Stabilizing a

*Corresponding author: greatkhan17@gmail.com

particular crystal structure through composition tuning is one clear benefit. To improve stability and effectiveness, it is necessary to increase the number of possible cation substitutions in these materials. This can be achieved with vacancy-ordered double perovskite halides A_2BX_6, in which every second B-site cation of the $A_2B_2X_6$ (i.e., doubled ABX_3) structure is removed [29].

Because of the interesting magnetic ordering and tunable electronic properties of double perovskites, some Cr-containing compositions, such as Nd_2FeCrO_6 and La_2CrCoO_6, have been reported as good candidates for spintronics [30]. Despite this progress, Cr-substituted lead-free double perovskites still lack detailed investigation, especially using a single approach to study their stability, magnetic ordering, electronic structure, thermoelectric properties, and optical properties [31]. In addition, studies that explore all these properties using a first-principles approach are relatively rare. Recent first-principles studies have shown that optical, electrical, and photovoltaic properties of double perovskites can be tuned by varying composition and engineering the electronic structure. In this regard, Zhang et al. studied the energy band gaps and electronic structures of $CsGeX_3$ (X=Cl, Br, I) materials in the visible range. Other optical properties of Cs_2SnI_6, including a 1.6 eV bandgap, were studied in terms of their applicability in photovoltaic devices [32]. Considerable progress has been made in applying halide double perovskites to solar energy harvesting [33]. Brik and Kityk modeled the lattice constants of an extensive group of A_2BX_6 cubic crystals (A = K, Cs, Rb, Tl; B = tetravalent cation; X = F, Cl, Br, I) in terms of the ionic radii and electronegativities of their constituent ions [34]. Halide perovskites are promising materials for thermoelectric devices and photovoltaics because of their environmentally friendly compositions. Motivated by these studies and by our previous first-principles work on halide double perovskites [35], the present work uses DFT to investigate the effect of 25% Cr substitution at the Ge site on the structural, electronic, magnetic, and thermoelectric properties of Cs_2GeX_6 (X = Cl, Br).

2. Methodology

DFT is a widely used method for computing the structural, electronic, and transport properties of crystals. We used the WIEN2k code [36], based on the full-potential linearized augmented plane wave plus local orbitals (FP-LAPW+lo) method, to calculate the properties of the undoped and Cr-doped compositions. The ground-state structural properties were determined by optimizing the unit-cell volume and relaxing the atomic positions, and the electronic and transport properties were then calculated using the optimized structural parameters. The Kohn–Sham equations were solved self-consistently within the WIEN2k package. Geometry optimization has been performed with GGA-PBE [37], and electronic structure calculations have been performed with the well-known modified Becke-Johnson (mBJ) exchange potential [38], which is known to produce much better predictions of band gaps of semiconductors and insulators than conventional GGA. The unit cell was divided into non-overlapping muffin-tin (MT) spheres around each atom and an interstitial region; within the MT spheres, the wave functions are expanded in atomic-like functions (radial functions multiplied by spherical harmonics), whereas plane waves are used in the interstitial region. For convergence, $l_{max} = 10$ and $R_{MT} \times K_{max} = 8$ were used, where R_{MT} is the smallest muffin-tin radius and K_{max} is the largest reciprocal-lattice vector in the plane-wave expansion. Spin-polarized calculations were performed for the Cr-doped compositions, which were modeled by replacing one of the four Ge atoms in the conventional cubic cell with Cr (25% doping). The transport properties were calculated with the BoltzTraP code [39] using a dense mesh of 4000 k-points.

3. Results and Discussion

3.1 Structural properties

This paper explores the structure of the halide double perovskite material A_2BX_6 (A = Cs; B = Ge; X = Cl, Br), which adopts a face-centered cubic structure with the space group Fm-3m (No. 225). Figures 1(a) and 1(b) show the crystal structures of pristine and Cr-doped A_2BX_6 (A = Cs; B = Ge; X = Cl, Br), i.e., the vacancy-ordered double perovskites Cs_2GeCl_6 and Cs_2GeBr_6 with Cr concentrations of 0% and 25% at the Ge site. Both structures are face-centered cubic, and the Fm-3m (No. 225) space group is employed throughout the calculations. The atomic positions Cs (0.25, 0.25, 0.25), Ge (0.00, 0.00, 0.00), and Cl/Br (0.20, 0.00, 0.00) are used [17], and Cr is introduced by substituting Ge, as shown in Figure 1(b). With increasing Cr concentration, the lattice parameters of Cs_2GeCl_6 and Cs_2GeBr_6 increase. The computed lattice parameters are: Cs_2GeCl_6: 10.32 Å, $Cs_2Ge_{0.75}Cr_{0.25}Cl_6$: 10.55 Å, Cs_2GeBr_6: 10.65 Å, and $Cs_2Ge_{0.75}Cr_{0.25}Br_6$: 10.85 Å. As shown in Figures 1(a) and 1(b), the structure can be viewed as a B-site-deficient ABX_3 perovskite built from BX_6 octahedra, with the A-site cations filling the cavities between the octahedra. Each $[BX_6]$ octahedron in the A_2BX_6 structure is isolated; each A-site cation is coordinated by 12 halide (Cl/Br) anions, whereas each B-site cation is octahedrally coordinated by 6 halide anions. The BX_6 octahedra are the essential building blocks of the cubic structure, and all structures remain cubic before and after doping. The optimized structural parameters obtained with GGA-PBE are listed in Table 1. To the best of our knowledge, no theoretical or experimental data are available for the Cr-doped compositions for comparison. The structural stability of the studied materials was further assessed using the Goldschmidt tolerance factor (t) and the octahedral factor (μ), defined as [40]:

$$\text{Tolerance factor} = t = \frac{r_A + r_X}{\sqrt{2}(r_B + r_X)} \quad (1)$$

$$\text{Octahedral factor} = \mu = \frac{r_B}{r_X} \quad (2)$$

Here, r_A, r_B, and r_X are the ionic radii of the A, B, and X ions in the ABX_3 perovskite structure. An ideal cubic

perovskite structure corresponds to t = 1, and the octahedral factor is an additional criterion describing the stability of the BX_6 octahedra. Both factors are empirical and neglect the chemical interactions between the constituents; consequently, the stability domain of ABX_3 depends on the chemical composition. For halide perovskites, the perovskite structure is generally expected to form when 0.813 < t < 1.107 and 0.442 < μ < 0.895. The estimation of tolerance and octahedral factors assumes that all ions, including the organic ones, are perfect hard spheres and that ionic radii do not depend on temperature. Nevertheless, these factors provide a simple and instructive estimate of perovskite stability. In the current work, perovskite crystal stability is estimated using both tolerance and octahedral criteria. These criteria were developed for ABX_3-type perovskites in which the A, B, and X ions have coordination numbers of 12, 6, and 6, respectively. The ionic radii of the B and X ions were taken from Shannon [41], whereas those of the A-site cations were adopted from the literature [42] because Shannon's tabulation does not provide complete data for 12-coordinated ions. The tolerance and octahedral factors were calculated using the values r_A= 1.88 Å, r_B= 0.73 Å, r_{Cl}= 1.81 Å, and r_{Br}=1.96 Å, r_{Cr}=0.80 Å [42]. The calculated values are: Cs_2GeCl_6: t= 1.02, μ= 0.40 and Cs_2GeBr_6: t= 1.01, μ= 0.37. The t values lie well within the stability range, indicating that the cubic structure is favored. The μ values are slightly below the lower limit of 0.442 established for ABX_3 perovskites; however, these ABX_3-based criteria are not directly transferable to vacancy-ordered A_2BX_6 compounds with isolated octahedra [6], and the stability of the studied structures is further supported by their negative formation energies (Table 1).

Table 1: Calculated lattice constant (a_o), bulk modulus (B_o), formation energy (ΔH_f), band gap (E_g), and total and atomic magnetic moments (M, in μ_B) of $Cs_2Ge_{1-x}Cr_xX_6$ (x= 0, 0.25).

Compound	a_o(Å)	B_o(GPa)	ΔH_f (eV)	E_g (eV)	M_{tot}	M_{Cr}	M_{Cs}	M_{Ge}	$M_{Cl/Br}$
Cs_2GeCl_6	10.32	64.31	-2.45	4.5	-	-	-	-	-
$Cs_2Ge_{0.75}Cr_{0.25}Cl_6$	10.55	52.16	-2.24	4.1	3.000	0.632	-0.009	0.2584	1.500
Cs_2GeBr_6	10.65	48.42	-2.30	3.0	-	-	-	-	-
$Cs_2Ge_{0.75}Cr_{0.25}Br_6$	10.85	36.46	-2.15	2.5	3.000	0.650	-0.007	0.2650	1.650

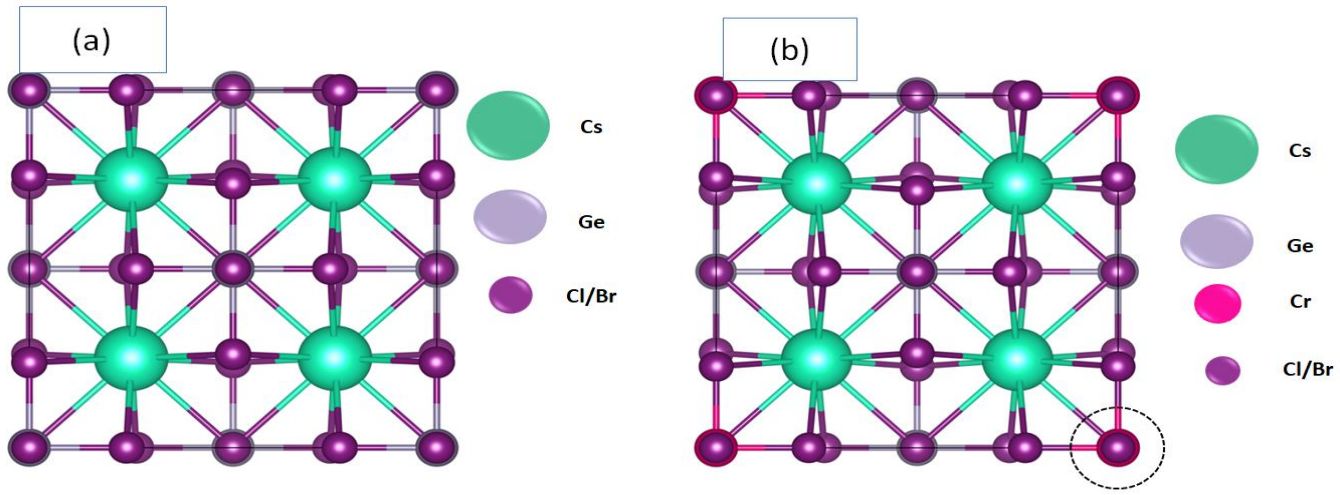


Fig. 1: Optimized cubic crystal structures of A_2BX_6: (a) pristine Cs_2GeX_6 and (b) $Cs_2Ge_{0.75}Cr_{0.25}X_6$ (A = Cs; B = Ge; X = Cl, Br); the substituted Cr site is circled

We used formation energies to study the thermodynamic stability of A_2BX_6 perovskites (A = Cs; B = Ge; X = Cl, Br). The formation energy is the difference between the total energy of the compound and the sum of the energies of its individual elemental constituents [43]. It is calculated as follows:

$$\Delta H_f = E_t^{A_2BX_6} - 2E_t^{A_{cubic}} - E_t^{B_{cubic}} - 6E_t^{X_{ortho}} \quad (3)$$

where $E_t^{A_2BX_6}$, E_t^A, E_t^B, and E_t^X denote the ground-state total energies of the A_2BX_6 compound and of the elemental constituents A, B, and X in their most stable standard structures, respectively; for the Cr-doped compositions, the corresponding term for elemental Cr is included. We carried out a comprehensive geometry optimization for each system under consideration, i.e., locating the volume at which the material's energy is lowest. When describing the stability of a compound, the sign and size of its formation energy are

most often cited in the literature. A negative formation energy indicates that the compound is thermodynamically stable with respect to its elemental constituents, whereas a positive value indicates instability, and a more negative formation energy corresponds to a more stable compound. The formation energies of all studied compounds are summarized in Table 1. All values are negative, indicating that the compounds are thermodynamically stable. Among the $Cs_2Ge_{1-x}Cr_xX_6$ (x = 0, 0.25) perovskites, Cs_2GeCl_6 is the most stable. After Cr doping, the stability of both Cs_2GeCl_6 and Cs_2GeBr_6 perovskites decreases slightly, although the Cr-doped chloride remains more stable than the Cr-doped bromide.

3.2 *Electronic properties*

To explain the electronic behavior, we studied the spin-polarized band structure, total density of states (TDOS), and partial density of states (PDOS) for $Cs_2Ge_{1-x}Cr_xX_6$ compounds at x = 0 and x = 0.25. The results of spin-dependent band structure and TDOS for both the spin-up and spin-down configurations are illustrated in Figures 2–4, where the spin-resolved PDOS is further decomposed into atomic and orbital contributions. The band gaps calculated with the mBJ potential are 4.5 eV for Cs_2GeCl_6, 4.1 eV for $Cs_2Ge_{0.75}Cr_{0.25}Cl_6$, 3.0 eV for Cs_2GeBr_6, and 2.5 eV for $Cs_2Ge_{0.75}Cr_{0.25}Br_6$.

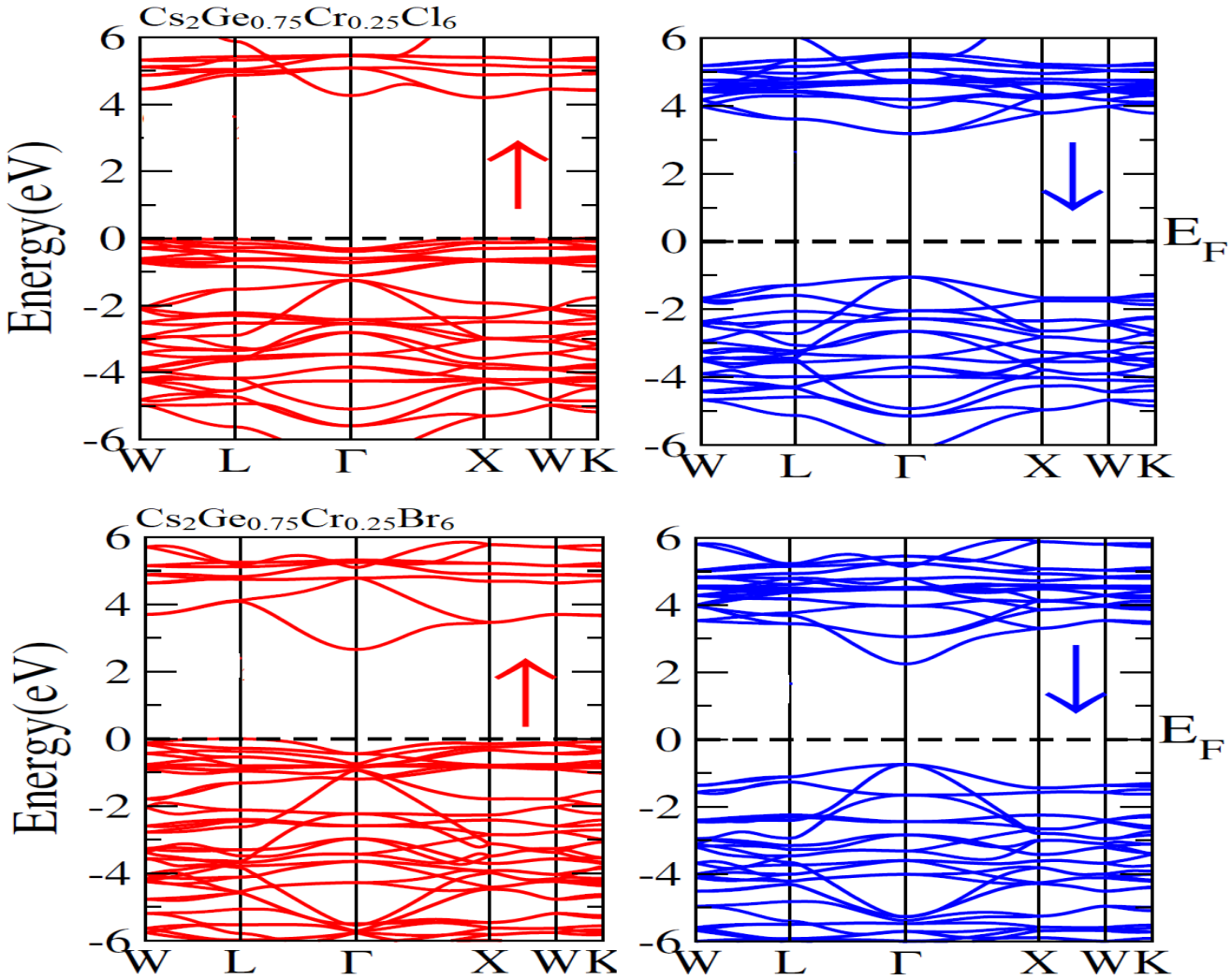


Fig. 2: Band structures of $Cs_2Ge_{0.75}Cr_{0.25}Cl_6$ and $Cs_2Ge_{0.75}Cr_{0.25}Br_6$ with up-spin and down-spin channels

The Fermi level (E_F) is set to 0 eV. The total and partial DOSs for the spin-up and spin-down channels were also computed with the mBJ potential. As shown in Figure 2, $Cs_2Ge_{0.75}Cr_{0.25}Cl_6$ and $Cs_2Ge_{0.75}Cr_{0.25}Br_6$ exhibit an indirect band gap in the spin-up channel, whereas in the spin-down channel both the valence band maximum (VBM) and the conduction band minimum (CBM) are located at the Γ point, giving a direct band gap. The band gap values of the four A_2BX_6 compounds studied are listed in Table 1.

Figure 2 shows the spin-polarized band structures of the Cr-doped A_2BX_6 perovskites calculated with the mBJ potential along the high-symmetry directions W–L–Γ–X–W–K of the Brillouin zone. Both doped compounds are semiconducting in both spin channels. For the 25% Cr-doped Cs_2GeCl_6/Br_6 compounds, the spin-up channel has an

indirect band gap owing to the nearly flat bands at the top of the valence band, whereas in the spin-down channel the VBM and CBM are both located at the Γ point (0, 0, 0).

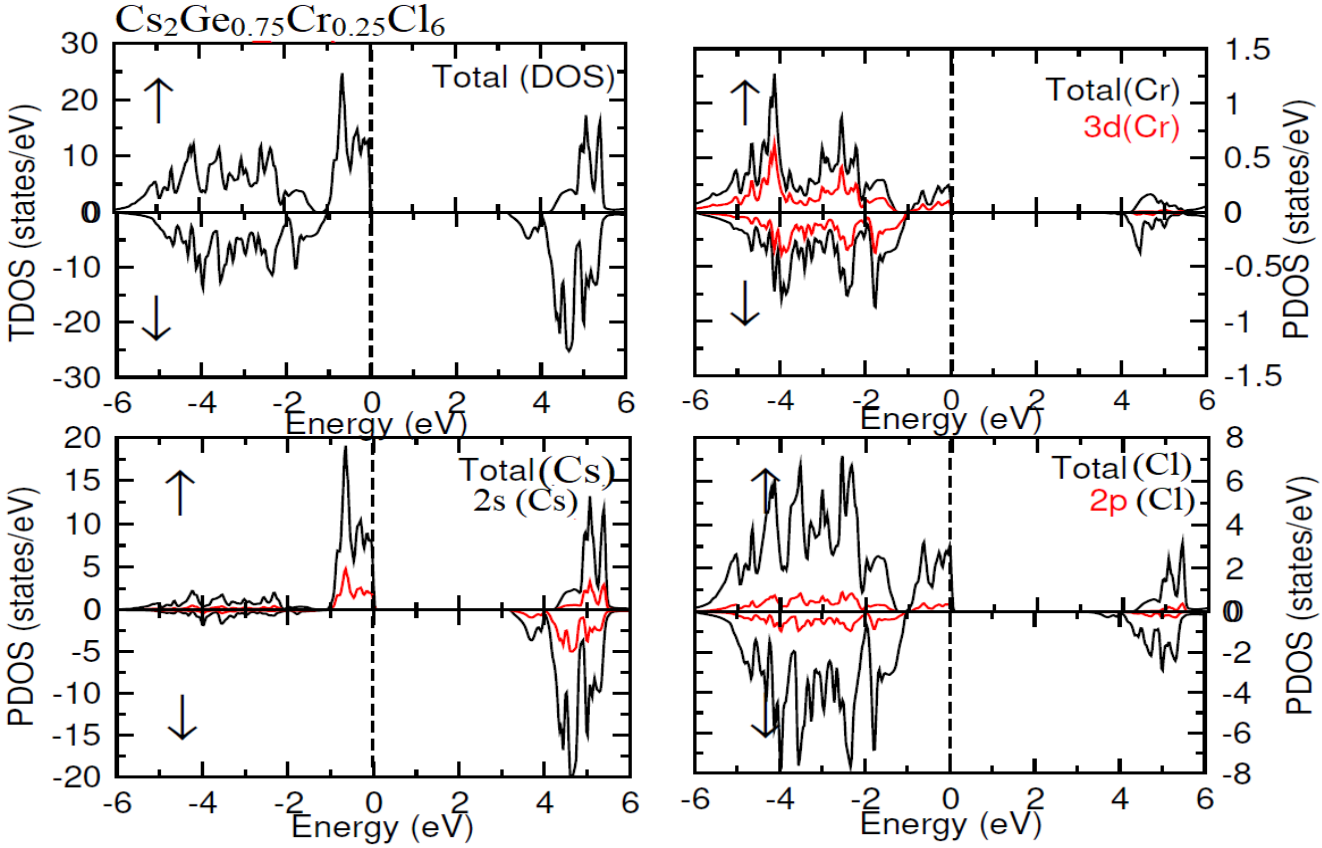


Fig. 3: Total and partial DOSs of $Cs_2Ge_{0.75}Cr_{0.25}Cl_6$ with up-spin and down-spin channels

Figures 3 and 4 show that the valence band is formed mainly by the halogen p states (Cl-3p/Br-4p), whereas the conduction band is dominated by Cs states with smaller halogen p contributions. In the TDOS and PDOS of $Cs_2Ge_{1-x}Cr_xX_6$ (x = 0, 0.25), the pronounced peaks between −1.5 and 6 eV indicate hybridization between the halogen p and Cs-s orbitals, and the significant hybridization of the Cs-s, Cr-3d, and halogen p orbitals produces the peaks just below the Fermi level. Cs_2GeCl_6 and Cs_2GeBr_6 are both semiconductors, and they remain semiconducting after 25% Cr substitution at the Ge site, as shown by the DOS plots. The PDOS of halide perovskites elucidates the role of each orbital in the band structures and reveals evidence of hybridization inside the double halide lead-free perovskites. Figures 3 and 4 show the PDOS (with 25% Cr doping) for $Cs_2Ge_{0.75}Cr_{0.25}Cl_6$ and $Cs_2Ge_{0.75}Cr_{0.25}Br_6$. The PDOS analysis suggests that the valence band maximum is mainly composed of contributions from the p states of Cl/Br, but also shows mixing with Cr-3d states, indicating strong covalent bonding between chromium and the halide elements. In contrast, the conduction band is dominated by Cs states with smaller halogen p contributions, while the Cr-3d contribution near the conduction-band edge is small. The energy range from −4 to 0 eV corresponds to the upper valence band, and the range above the band gap corresponds to the lower conduction band. As seen in Figures 3 and 4, the halogen (Cl/Br) p states in both spin channels are the dominant contributors to the upper valence band, whereas their contribution to the conduction-band edge is smaller. Incorporating Cr creates localized 3d electronic states that strongly hybridize with neighboring anion p-orbitals, changing the electronic band dispersion near the Fermi level. Hybridization decreases the band gap and increases spin polarization, which is desired for spintronics. It has also been discussed that the extent of band-gap modification depends on the exchange interaction and crystal-field splitting of Cr 3d states [44].

3.3 Magnetic properties

The total and atom-resolved magnetic moments (M_{tot}, M_{Cs}, $M_{Cl/Br}$, M_{Ge}, M_{Cr}) are listed in Table 1. Figures 2, 3, and 4 show the band structures, TDOS, and PDOS for $Cs_2Ge_{0.75}Cr_{0.25}Cl_6$ and $Cs_2Ge_{0.75}Cr_{0.25}Br_6$. We then evaluate the magnetic moment using the GGA + mBJ potential approach and discuss the atomic contributions. Both doped compounds have an integer total magnetic moment of 3 μ_B per unit cell within the GGA + mBJ scheme, which is characteristic of ferromagnetic semiconductors. The relatively large contribution of the halogen atoms ($M_{Cl/Br}$) to the total moment reflects the spin-polarized halogen p states hybridized with the Cr-3d states [45]. The small contributions of the Cs and Ge atoms reflect their states

lying far from the Fermi level, whereas the Cl and Br states are prominent near the Fermi level, as reflected in the PDOS calculated with the GGA + mBJ scheme. Table 1 shows the results of our calculations for the total and individual magnetic moments of the atoms.

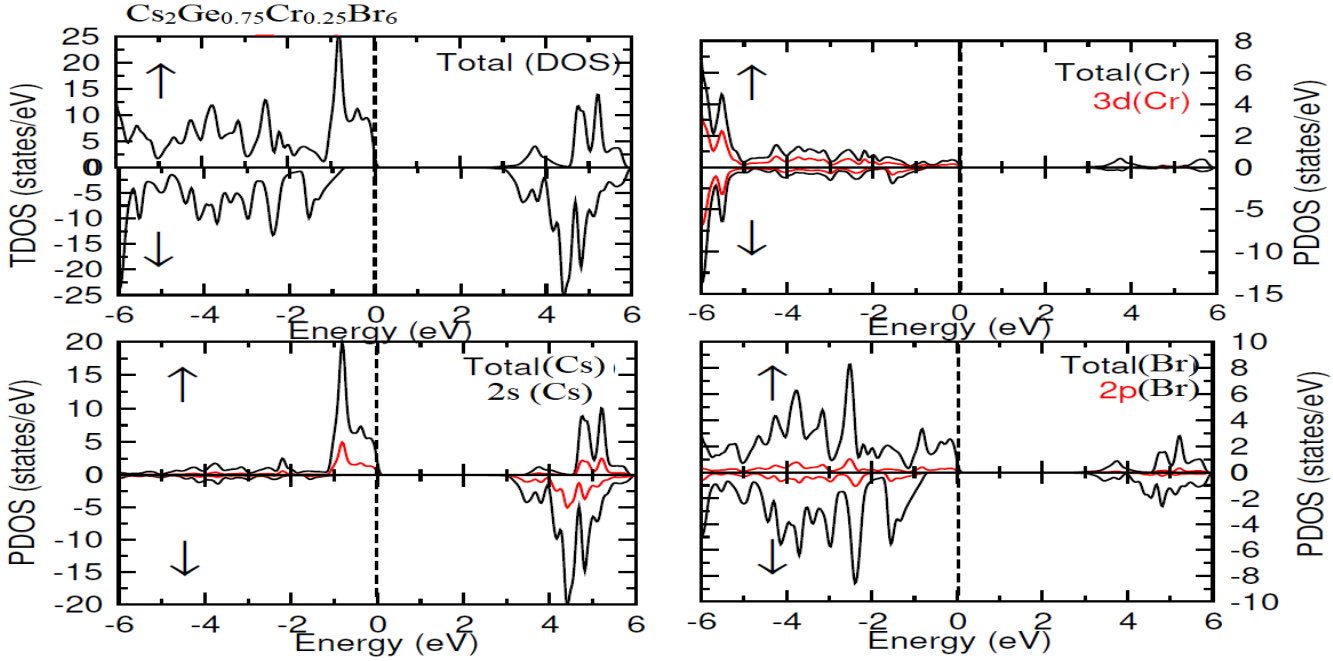


Fig. 4: TDOS and PDOS of $Cs_2Ge_{0.75}Cr_{0.25}Br_6$ with up-spin and down-spin channels

3.4 Thermoelectric properties

The band structure determines the thermoelectric behavior of a material, which makes band-gap engineering an effective tool for tuning it. Thermoelectric (TE) materials convert waste heat directly into electrical energy, and because of this energy-conversion capability they are currently attracting intense research interest [46]. The thermoelectric transport properties were calculated using the BoltzTraP code [39], which solves the semiclassical Boltzmann transport equations in the constant relaxation time approximation (CRTA). These calculations use the band structure data obtained from the first-principles calculations, where an energy-independent relaxation time (τ) is used, along with the rigid band approximation to account for doping effects. In such a case, the Seebeck coefficient (S) does not depend on τ, whereas the electrical conductivity (σ) and electronic thermal conductivity (κ_e) are obtained only as the ratios σ/τ and κ_e/τ, respectively. Within this approach, scattering mechanisms are not treated explicitly. The thermopower (Seebeck coefficient) is the electromotive force generated per unit temperature difference across a material; it is a key indicator of thermoelectric performance and is governed by the electronic band structure [47]. The thermoelectric efficiency is quantified by the dimensionless figure of merit ZT = $S^2\sigma T/\kappa$, where $\kappa = \kappa_l + \kappa_{el}$ is the total thermal conductivity, i.e., the sum of the lattice (κ_l) and electronic (κ_{el}) contributions. Optimizing these transport parameters requires an understanding of electron and phonon transport in TE materials. In terms of Boltzmann transport theory, a number of transport coefficients, namely, the electrical conductivity, Seebeck coefficient, electronic thermal conductivity, and power factor, have been calculated to study the electronic transport characteristics of the $Cs_2Ge_{1-x}Cr_xX_6$ (x = 0, 0.25) perovskites within the assumptions of the constant relaxation time and rigid band approximations [48]. These transport coefficients include electrical conductivity (σ/τ), Seebeck coefficient (S), and electronic thermal conductivity (κ_e/τ). The results are shown in Figures 5 and 6.

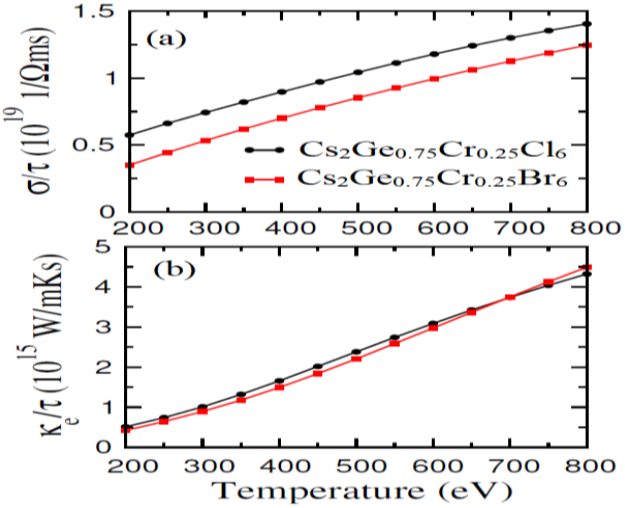


Fig. 5: (a) Electrical conductivity (σ/τ) and (b) electronic thermal conductivity (κ_e/τ) of $Cs_2Ge_{0.75}Cr_{0.25}Cl_6$ and $Cs_2Ge_{0.75}Cr_{0.25}Br_6$

A compound is p- or n-type depending on whether holes in the valence band or electrons in the conduction band are

the majority charge carriers. When calculating the thermoelectric characteristics of $Cs_2Ge_{1-x}Cr_xX_6$ (x = 0, 0.25) double perovskites, the BoltzTraP code is employed (see Section 2). The electrical conductivity of $Cs_2Ge_{0.75}Cr_{0.25}Cl_6$ and $Cs_2Ge_{0.75}Cr_{0.25}Br_6$ is shown in Figure 5(a). At 200 K, the values obtained from Figure 5(a) are, for $Cs_2Ge_{0.75}Cr_{0.25}Cl_6$, $\sigma/\tau = 0.60 \times 10^{19}(\Omega ms)^{-1}$ and for $Cs_2Ge_{0.75}Cr_{0.25}Br_6$, $\sigma/\tau = 0.30 \times 10^{19}(\Omega ms)^{-1}$. The electrical conductivity increases with temperature because more carriers are thermally excited at higher temperatures. At 800 K, the values are, for $Cs_2Ge_{0.75}Cr_{0.25}Cl_6$, $\sigma/\tau = 1.40 \times 10^{19}(\Omega ms)^{-1}$ and for $Cs_2Ge_{0.75}Cr_{0.25}Br_6$, $\sigma/\tau = 1.25 \times 10^{19}(\Omega ms)^{-1}$. Heat is conducted by both electrons and phonons, so the thermal conductivity is given by $\kappa = \kappa_{electron} + \kappa_{phonon}$, where κ_{phonon} and $\kappa_{electron}$ are the phononic and electronic thermal conductivity coefficients, respectively. Because BoltzTraP evaluates only the electronic part, only the electronic contribution to the thermal conductivity is considered here, and the lattice (phonon) contribution is neglected [49]. Figure 5(b) shows the calculated electronic thermal conductivity. At 200 K, the values are, for $Cs_2Ge_{0.75}Cr_{0.25}Cl_6$, $\kappa_{electron}/\tau = 0.50 \times 10^{15} W/Kms$ and for $Cs_2Ge_{0.75}Cr_{0.25}Br_6$, $\kappa_{electron}/\tau = 0.40 \times 10^{15} W/Kms$. As seen in Figure 5(b), κ_e/τ increases rapidly with temperature. At 800 K, the values are, for $Cs_2Ge_{0.75}Cr_{0.25}Cl_6$, $\kappa_{electron}/\tau = 4.40 \times 10^{15} W/Kms$ and for $Cs_2Ge_{0.75}Cr_{0.25}Br_6$, $\kappa_{electron}/\tau = 4.50 \times 10^{15} W/Kms$. This increase follows that of the electrical conductivity, as expected from the Wiedemann–Franz law. Overall, the calculated values suggest that the studied materials can be used for thermoelectric devices.

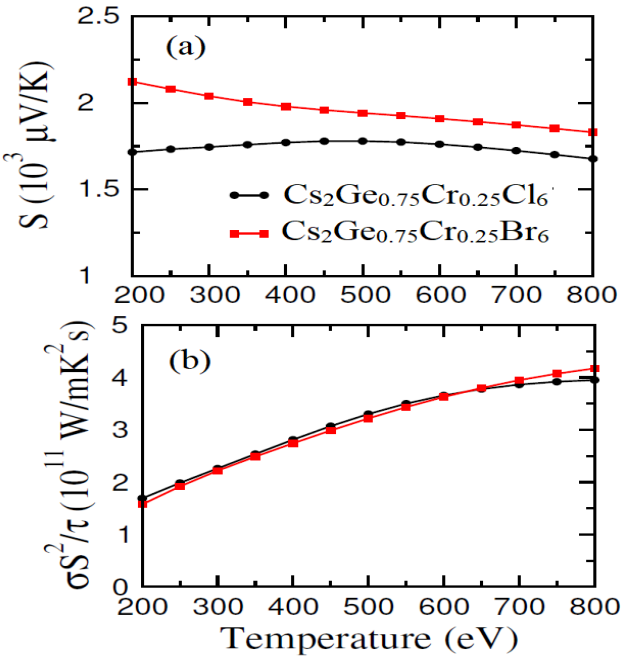


Fig. 6: (a) Seebeck coefficient (S) and (b) power factor ($\sigma S^2/\tau$) of $Cs_2Ge_{0.75}Cr_{0.25}Cl_6$ and $Cs_2Ge_{0.75}Cr_{0.25}Br_6$

In a thermoelectric system, the temperature difference between two junctions of dissimilar conductors creates a voltage difference, and the Seebeck coefficient, S, determines its effect on device efficiency. As shown in Fig. 6(a), the Seebeck coefficient of $Cs_2Ge_{0.75}Cr_{0.25}Br_6$ decreases monotonically with temperature over 200–800 K, whereas that of $Cs_2Ge_{0.75}Cr_{0.25}Cl_6$ increases slightly up to about 500 K and then decreases; the decrease at high temperatures is attributed to the thermal excitation of additional carriers. The positive sign of S indicates that both materials are p-type semiconductors in which holes are responsible for charge transport. It can be noted that the values of the thermoelectric parameters found are consistent with the electronic structure. The large value of the Seebeck coefficient comes from the semiconducting nature of the materials, as well as the presence of the sharp density of states peaks at the band edges. Electrical conductivity depends on the dispersion of the bands near the Fermi level; the larger the dispersion, the higher the conductivity.

It should be noted that the temperature dependence of the electronic thermal conductivity corresponds to the dependence of electrical conductivity, since both are associated with charge-carrier motion according to the Wiedemann-Franz law. Computed Seebeck coefficients of $Cs_2Ge_{0.75}Cr_{0.25}Cl_6$ and $Cs_2Ge_{0.75}Cr_{0.25}Br_6$ at 200 K are 1.73 × 10^3 and 2.13 × 10^3 μV/K, respectively. At 800 K, these materials yield Seebeck coefficients of 1.70 × 10^3 μV/K and 1.80 × 10^3 μV/K for $Cs_2Ge_{0.75}Cr_{0.25}Cl_6$ and $Cs_2Ge_{0.75}Cr_{0.25}Br_6$, respectively. The material $Cs_2Ge_{0.75}Cr_{0.25}Br_6$ has relatively large Seebeck coefficients compared with those of $Cs_2Ge_{0.75}Cr_{0.25}Cl_6$, which is consistent with its lower electrical conductivity (Figure 5(a)) and reflects the usual inverse relationship between S and σ. In thermoelectricity, two main parameters determine a material's efficiency in energy generation: electrical conductivity and the Seebeck coefficient, commonly represented by the power factor ($PF/\tau = S^2\sigma/\tau$). The temperature dependence of the power factor is shown in Fig. 6(b). The PF/τ of both compounds increases almost linearly from 200 to 650 K; above 650 K, it continues to increase for $Cs_2Ge_{0.75}Cr_{0.25}Br_6$, whereas it tends to saturate for $Cs_2Ge_{0.75}Cr_{0.25}Cl_6$. The calculated PF/τ values of $Cs_2Ge_{0.75}Cr_{0.25}Cl_6$ and $Cs_2Ge_{0.75}Cr_{0.25}Br_6$ at 200 K are $1.90\times 10^{11} W/K^2ms$ and $1.85 \times 10^{11} W/K^2ms$, respectively. At 800 K, the values are $3.98\times 10^{11} W/K^2ms$ for $Cs_2Ge_{0.75}Cr_{0.25}Cl_6$ and $4.09\times 10^{11} W/K^2ms$ for $Cs_2Ge_{0.75}Cr_{0.25}Br_6$. Additionally, the room-temperature ZT was calculated using $ZT = \sigma S^2T/\kappa$, giving values of 0.79 and 0.78 for $Cs_2Ge_{0.75}Cr_{0.25}Cl_6$ and $Cs_2Ge_{0.75}Cr_{0.25}Br_6$, respectively, which indicates that both doped compositions are promising for thermoelectric devices. Because the lattice thermal conductivity is neglected, these ZT values should be regarded as upper limits.

4. Conclusions

In the current research, density functional theory (DFT) within the FP-LAPW+lo method was applied to investigate the structural, electronic, magnetic, and thermoelectric properties of pristine and 25% Cr-doped A_2BX_6 (A = Cs, B = Ge, X = Cl, Br) halides. The results indicate that the

equilibrium lattice parameters of Cs_2GeCl_6 and Cs_2GeBr_6 increase with Cr doping, with computed values of Cs_2GeCl_6: 10.32 Å, $Cs_2Ge_{0.75}Cr_{0.25}Cl_6$: 10.55 Å, Cs_2GeBr_6: 10.65 Å, and $Cs_2Ge_{0.75}Cr_{0.25}Br_6$: 10.85 Å. The negative formation energies and the tolerance factors confirm the thermodynamic and structural stability of the compounds. The computed band gap of Cs_2GeCl_6 is 4.5 eV, that of $Cs_2Ge_{0.75}Cr_{0.25}Cl_6$ is 4.1 eV, that of Cs_2GeBr_6 is 3.0 eV, and that of $Cs_2Ge_{0.75}Cr_{0.25}Br_6$ is 2.5 eV. $Cs_2Ge_{0.75}Cr_{0.25}Cl_6$ and $Cs_2Ge_{0.75}Cr_{0.25}Br_6$ exhibit an indirect band gap in the spin-up channel and a direct band gap in the spin-down channel. With 25% Cr doping, the total magnetic moments of $Cs_2Ge_{0.75}Cr_{0.25}Cl_6$ and $Cs_2Ge_{0.75}Cr_{0.25}Br_6$ are identical (3 μ_B), indicating ferromagnetic semiconducting behavior of interest for spintronic applications. The room-temperature figure of merit is calculated to be 0.79 for $Cs_2Ge_{0.75}Cr_{0.25}Cl_6$ and 0.78 for $Cs_2Ge_{0.75}Cr_{0.25}Br_6$, indicating that these compounds are promising thermoelectric materials, and the positive Seebeck coefficients confirm p-type conduction.

References

[1] Q. A. Akkerman and L. Manna, "What defines a halide perovskite?" *ACS Energy Lett.*, vol. 5, no. 2, pp. 604–610, 2020, doi: 10.1021/acsenergylett.0c00039.

[2] Q. Tai, K. C. Tang, and F. Yan, "Recent progress of inorganic perovskite solar cells," *Energy Environ. Sci.*, vol. 12, pp. 2375–2405, 2019, doi: 10.1039/C9EE01479A.

[3] R. Wang, M. Mujahid, Y. Duan, Z. K. Wang, J. Xue, and Y. Yang, "A review of perovskites solar cell stability," *Adv. Funct. Mater.*, vol. 29, Art. no. 1808843, 2019, doi: 10.1002/adfm.201808843.

[4] J. Zhang, Z. Zhao, Z. Xia, and L. Dai, "A metal-free bifunctional electrocatalyst for oxygen reduction and oxygen evolution reactions," *Nat. Nanotechnol.*, vol. 10, pp. 444–452, 2015, doi: 10.1038/nnano.2015.48.

[5] T. R. Cook, D. K. Dogutan, S. Y. Reece, Y. Surendranath, T. S. Teets, and D. G. Nocera, "Solar energy supply and storage for the legacy and nonlegacy worlds," *Chem. Rev.*, vol. 110, no. 11, pp. 6474–6502, 2010, doi: 10.1021/cr100246c.

[6] A. E. Fedorovskiy, N. A. Drigo, and M. K. Nazeeruddin, "The role of Goldschmidt's tolerance factor in the formation of A_2BX_6 double halide perovskites and its optimal range," *Small Methods*, vol. 4, Art. no. 1900426, 2020, doi: 10.1002/smtd.201900426.

[7] G. Catalan and J. F. Scott, "Physics and applications of bismuth ferrite," *Adv. Mater.*, vol. 21, pp. 2463–2485, 2009, doi: 10.1002/adma.200802849.

[8] M.-G. Ju, M. Chen, Y. Zhou, H. F. Garces, J. Dai, L. Ma, N. P. Padture, and X. C. Zeng, "Earth-abundant nontoxic titanium(IV)-based vacancy-ordered double perovskite halides with tunable 1.0 to 1.8 eV bandgaps for photovoltaic applications," *ACS Energy Lett.*, vol. 3, pp. 297–304, 2018, doi: 10.1021/acsenergylett.7b01167.

[9] P. K. Kung, M. H. Li, P. Y. Lin, J. Y. Jhang, M. Pantaler, D. C. Lupascu, G. Grancini, and P. Chen, "Lead-free double perovskites for perovskite solar cells," *Sol. RRL*, vol. 4, Art. no. 1900306, 2020, doi: 10.1002/solr.201900306.

[10] S. Thawarkar, S. R. Rondiya, N. Y. Dzade, N. Khupse, and S. Jadkar, "Experimental and theoretical investigation of the structural and opto-electronic properties of Fe-doped lead-free $Cs_2AgBiCl_6$ double perovskite," *Chem. Eur. J.*, vol. 27, pp. 7408–7417, 2021, doi: 10.1002/chem.202004902.

[11] A. Kojima, K. Teshima, Y. Shirai, and T. Miyasaka, "Organometal halide perovskites as visible-light sensitizers for photovoltaic cells," *J. Am. Chem. Soc.*, vol. 131, pp. 6050–6051, 2009, doi: 10.1021/ja809598r.

[12] W. Xu *et al.*, "Rational molecular passivation for high-performance perovskite light-emitting diodes," *Nat. Photonics*, vol. 13, pp. 418–424, 2019, doi: 10.1038/s41566-019-0390-x.

[13] L. Chu, W. Ahmad, W. Liu, J. Yang, R. Zhang, Y. Sun, J. Yang, and X. Li, "Lead-free halide double perovskite materials: A new superstar toward green and stable optoelectronic applications," *Nano-Micro Lett.*, vol. 11, Art. no. 16, 2019, doi: 10.1007/s40820-019-0244-6.

[14] M. I. Khan *et al.*, "Investigations on the efficiency variation of zinc and gallium co-doped TiO_2 based dye sensitized solar cells," *Ceram. Int.*, vol. 46, pp. 24844–24849, 2020, doi: 10.1016/j.ceramint.2020.06.268.

[15] Q. Mahmood *et al.*, "The study of optical and thermoelectric properties of lead-free variant iodides $(K/Rb)_2TiI_6$," *J. Mater. Res. Technol.*, vol. 9, pp. 13043–13053, 2020, doi: 10.1016/j.jmrt.2020.09.046.

[16] R. Ali, G. J. Hou, Z. G. Zhu, Q. B. Yan, Q. R. Zheng, and G. Su, "Predicted lead-free perovskites for solar cells," *Chem. Mater.*, vol. 30, pp. 718–728, 2018, doi: 10.1021/acs.chemmater.7b04036.

[17] T. I. Al-Muhimeed *et al.*, "New lead-free double perovskites X_2GeI_6 (X = K, Rb, Cs) for solar cells, and renewable energy as an alternate of hybrid perovskites," *Int. J. Energy Res.*, vol. 45, no. 13, pp. 19645–19652, 2021, doi: 10.1002/er.7022.

[18] G. Flora, D. Gupta, and A. Tiwari, "Toxicity of lead: A review with recent updates," *Interdiscip. Toxicol.*, vol. 5, pp. 47–58, 2012, doi: 10.2478/v10102-012-0009-2.

[19] S. Berri, "Thermoelectric properties of A_2BCl_6: A first-principles study," *J. Phys. Chem. Solids*, vol. 170, Art. no. 110940, 2022, doi: 10.1016/j.jpcs.2022.110940.

[20] F. Hao, C. C. Stoumpos, R. P. H. Chang, and M. G. Kanatzidis, "Anomalous band gap behavior in mixed Sn and Pb perovskites enables broadening of absorption spectrum in solar cells," *J. Am. Chem. Soc.*, vol. 136, pp. 8094–8099, 2014, doi: 10.1021/ja5033259.

[21] T. Krishnamoorthy *et al.*, "Lead-free germanium iodide perovskite materials for photovoltaic applications," *J. Mater. Chem. A*, vol. 3, pp. 23829–23832, 2015, doi: 10.1039/C5TA05741H.

[22] J. C. Hebig, I. Kühn, J. Flohre, and T. Kirchartz, "Optoelectronic properties of $(CH_3NH_3)_3Sb_2I_9$ thin films for photovoltaic applications," *ACS Energy Lett.*, vol. 1, pp. 309–314, 2016, doi: 10.1021/acsenergylett.6b00170.

[23] T. Singh, A. Kulkarni, M. Ikegami, and T. Miyasaka, "Effect of electron transporting layer on bismuth-based lead-free perovskite $(CH_3NH_3)_3Bi_2I_9$ for photovoltaic applications," *ACS Appl. Mater. Interfaces*, vol. 8, pp. 14542–14547, 2016, doi: 10.1021/acsami.6b02843.

[24] M. T. Klug *et al.*, "Tailoring metal halide perovskites through metal substitution: Influence on photovoltaic and material properties," *Energy Environ. Sci.*, vol. 10, pp. 236–246, 2017, doi: 10.1039/C6EE03201J.

[25] Y. Hu, T. Qiu, F. Bai, X. Miao, and S. Zhang, "Enhancing moisture-tolerance and photovoltaic performances of $FAPbI_3$ by bismuth incorporation," *J. Mater. Chem. A*, vol. 5, pp. 25258–25265, 2017, doi: 10.1039/C7TA08824H.

[26] M. A. Green, A. Ho-Baillie, and H. J. Snaith, "The emergence of perovskite solar cells," *Nat. Photonics*, vol. 8, pp. 506–514, 2014, doi: 10.1038/nphoton.2014.134.

[27] M. Saliba *et al.*, "A molecularly engineered hole-transporting material for efficient perovskite solar cells," *Nat. Energy*, vol. 1, Art. no. 15017, 2016, doi: 10.1038/nenergy.2015.17.

[28] V. Malgras, A. Nattestad, J. H. Kim, S. X. Dou, and Y. Yamauchi, "Understanding chemically processed solar cells based on quantum dots," *Sci. Technol. Adv. Mater.*, vol. 18, pp. 334–350, 2017, doi: 10.1080/14686996.2017.1317219.

[29] A. E. Maughan, A. M. Ganose, M. M. Bordelon, E. M. Miller, D. O. Scanlon, and J. R. Neilson, "Defect tolerance to intolerance in the vacancy-ordered double perovskite semiconductors Cs_2SnI_6 and Cs_2TeI_6," *J. Am. Chem. Soc.*, vol. 138, pp. 8453–8464, 2016, doi: 10.1021/jacs.6b03207.

[30] M. D. I. Bhuyan, R. Hossain, F. Ara, and M. A. Basith, "A first-principles study on the phase stability and physical properties of a B-

site ordered Nd_2CrFeO_6 double perovskite," *Phys. Chem. Chem. Phys.*, vol. 24, pp. 1569–1579, 2022.

[31] Kumawat, M. Rani, D. K. Meena, Anuradha, K. Kumar, and G. Arora, "Electronic, optical and magnetic properties of Gd_2FeCrO_6 double perovskite using DFT," *Mater. Today Proc.*, 2023.

[32] Q. Mahmood, T. Ghrib, A. Rached, A. Laref, and M. A. Kamran, "Probing of mechanical, optical and thermoelectric characteristics of double perovskites Cs_2GeCl/Br_6 by DFT method," *Mater. Sci. Semicond. Process.*, vol. 112, Art. no. 105009, 2020, doi: 10.1016/j.mssp.2020.105009.

[33] M. Faizan *et al.*, "Electronic, optical, and thermoelectric properties of perovskite variants A_2BX_6: Insight and design via first-principles calculations," *Int. J. Energy Res.*, vol. 45, pp. 4495–4507, 2021, doi: 10.1002/er.6118.

[34] M. G. Brik and I. V. Kityk, "Modeling of lattice constant and their relations with ionic radii and electronegativity of constituting ions of A_2XY_6 cubic crystals (A = K, Cs, Rb, Tl; X = tetravalent cation, Y = F, Cl, Br, I)," *J. Phys. Chem. Solids*, vol. 72, pp. 1256–1260, 2011, doi: 10.1016/j.jpcs.2011.07.016.

[35] M. Asghar, M. Zanib, M. A. Khan, S. Niaz, N. A. Noor, and A. Dahshan, "Tuning of the bandgap of Rb_2ScAgX_6 (X = Cl, Br, I) double perovskites through halide ion replacement for solar cell applications," *Mater. Sci. Semicond. Process.*, vol. 148, Art. no. 106819, 2022, doi: 10.1016/j.mssp.2022.106819.

[36] P. Blaha, K. Schwarz, G. K. H. Madsen, D. Kvasnicka, and J. Luitz, *WIEN2k: An Augmented Plane Wave + Local Orbitals Program for Calculating Crystal Properties*. Vienna, Austria: Vienna Univ. Technol., 2001.

[37] J. P. Perdew, K. Burke, and M. Ernzerhof, "Generalized gradient approximation made simple," *Phys. Rev. Lett.*, vol. 77, no. 18, pp. 3865–3868, 1996, doi: 10.1103/PhysRevLett.77.3865.

[38] F. Tran and P. Blaha, "Accurate band gaps of semiconductors and insulators with a semilocal exchange-correlation potential," *Phys. Rev. Lett.*, vol. 102, no. 22, Art. no. 226401, 2009, doi: 10.1103/PhysRevLett.102.226401.

[39] G. K. H. Madsen and D. J. Singh, "BoltzTraP. A code for calculating band-structure dependent quantities," *Comput. Phys. Commun.*, vol. 175, no. 1, pp. 67–71, 2006, doi: 10.1016/j.cpc.2006.03.007.

[40] V. M. Goldschmidt, "Die Gesetze der Krystallochemie," *Naturwissenschaften*, vol. 14, no. 21, pp. 477–485, 1926, doi: 10.1007/BF01507527.

[41] R. D. Shannon, "Revised effective ionic radii and systematic studies of interatomic distances in halides and chalcogenides," *Acta Crystallogr. A*, vol. 32, no. 5, pp. 751–767, 1976, doi: 10.1107/S0567739476001551.

[42] H. Tanaka, T. Oku, and N. Ueoka, "Structural stabilities of organic–inorganic perovskite crystals," *Jpn. J. Appl. Phys.*, vol. 57, no. 8S3, Art. no. 08RE12, 2018, doi: 10.7567/JJAP.57.08RE12.

[43] A. Zunger, "Practical doping principles," *Appl. Phys. Lett.*, vol. 83, no. 1, pp. 57–59, 2003, doi: 10.1063/1.1584074.

[44] V. I. Anisimov, J. Zaanen, and O. K. Andersen, "Band theory and Mott insulators: Hubbard U instead of Stoner I," *Phys. Rev. B*, vol. 44, no. 3, pp. 943–954, 1991, doi: 10.1103/PhysRevB.44.943.

[45] S. A. Mir and D. C. Gupta, "Systematic investigation of the magneto-electronic structure and optical properties of new halide double perovskites Cs_2NaMCl_6 (M = Mn, Co and Ni) by spin polarized calculations," *RSC Adv.*, vol. 10, no. 44, pp. 26277–26287, 2020.

[46] H. Rached, S. Bendaoudia, and D. Rached, "Investigation of iron-based double perovskite oxides on the magnetic phase stability, mechanical, electronic and optical properties via first-principles calculation," *Mater. Chem. Phys.*, vol. 193, pp. 453–469, 2017.

[47] M. Fatmi *et al.*, "High performance double perovskites of $Cs_2InAgBr_6$ and $Cs_2InAgCl_6$ structural electronic optical and thermoelectric properties for next-generation photovoltaics," *Sci. Rep.*, vol. 15, no. 1, Art. no. 20851, 2025.

[48] J. Kanamori, "Superexchange interaction and symmetry properties of electron orbitals," *J. Phys. Chem. Solids*, vol. 10, no. 2–3, pp. 87–98, 1959, doi: 10.1016/0022-3697(59)90061-7.

[49] U. Singh, J. Klarbring, I. A. Abrikosov, and S. I. Simak, "Exploring magnetism of lead-free halide double perovskites: A high-throughput first-principles study," *Phys. Rev. Mater.*, vol. 7, no. 11, Art. no. 114404, 2023.